Figure S1

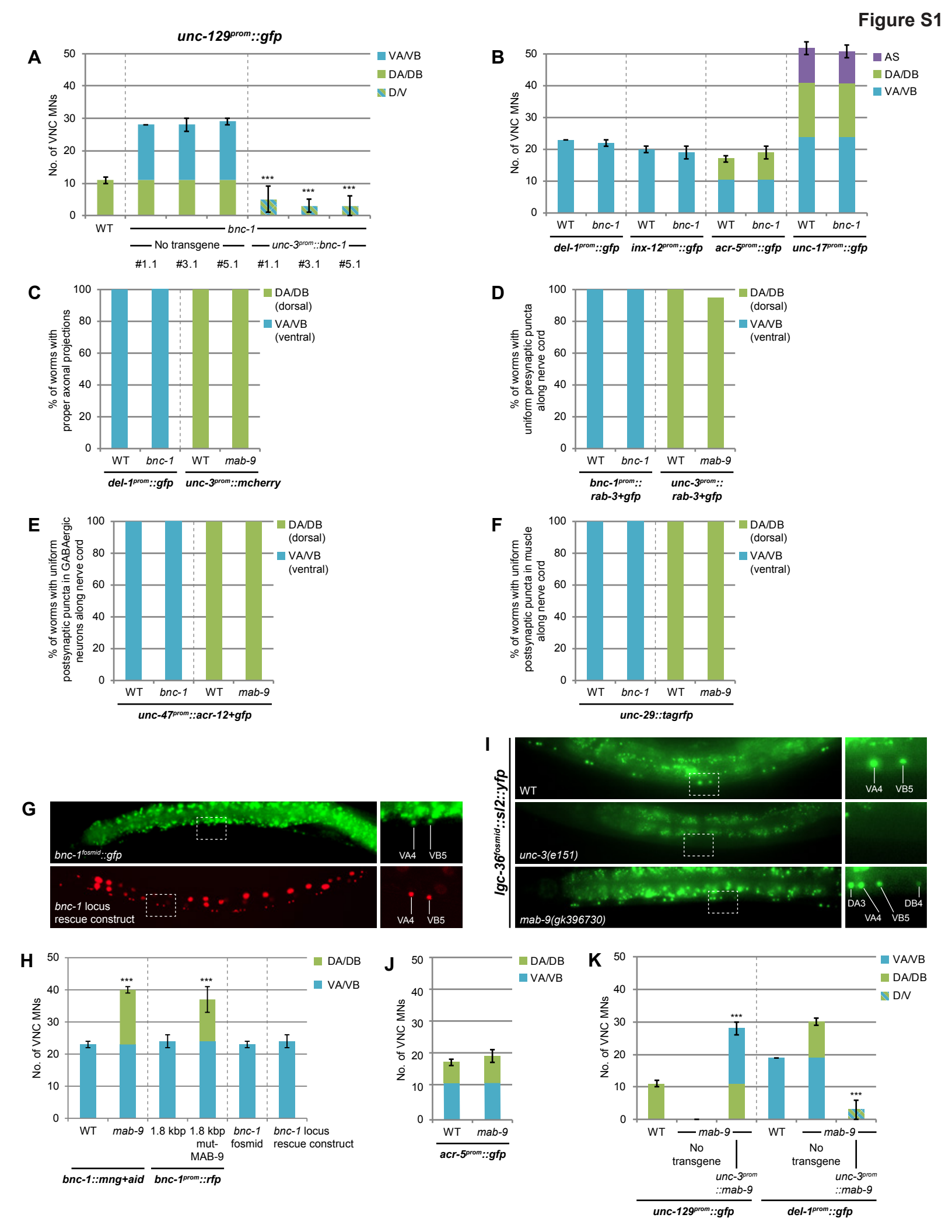
A
unc-129prom::gfp
No. of VNC MNs
VA/VB
DA/DB
D/V
WT
bnc-1
No transgene
unc-3prom::bnc-1
#1.1
#3.1
#5.1
B
AS
DA/DB
VA/VB
del-1prom::gfp
inx-12prom::gfp
acr-5prom::gfp
unc-17prom::gfp
C
% of worms with proper axonal projections
DA/DB (dorsal)
VA/VB (ventral)
mab-9
unc-3prom::mcherry
D
% of worms with uniform presynaptic puncta along nerve cord
bnc-1prom:: rab-3+gfp
unc-3prom:: rab-3+gfp
E
% of worms with uniform postsynaptic puncta in GABAergic neurons along nerve cord
unc-47prom::acr-12+gfp
F
% of worms with uniform postsynaptic puncta in muscle along nerve cord
unc-29::tagrfp
G
bnc-1fosmid::gfp
VA4
VB5
bnc-1 locus rescue construct
I
lgc-36fosmid::sl2::yfp
WT
unc-3(e151)
mab-9(gk396730)
DA3
DB4
H
1.8 kbp
1.8 kbp mut-MAB-9
bnc-1 fosmid
bnc-1 locus rescue construct
bnc-1::mng+aid
bnc-1prom::rfp
J
acr-5prom::gfp
K
No transgene
unc-3prom ::mab-9
unc-129prom::gfp
del-1prom::gfp

Figure S2

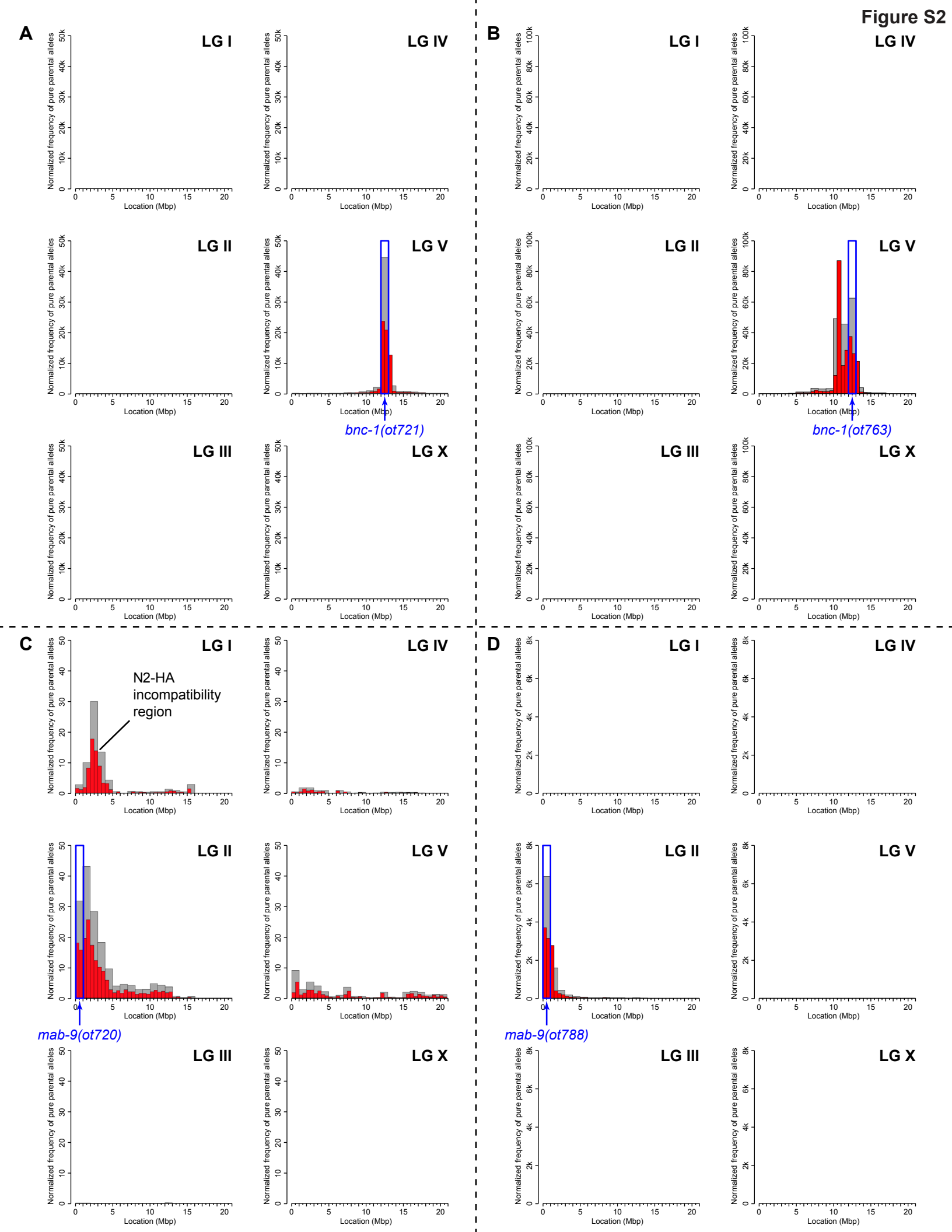
A
B
C
D
LG I
LG II
LG III
LG IV
LG V
LG X
Normalized frequency of pure parental alleles
Location (Mbp)
bnc-1(ot721)
bnc-1(ot763)
N2-HA incompatibility region
mab-9(ot720)
mab-9(ot788)

Figure S3

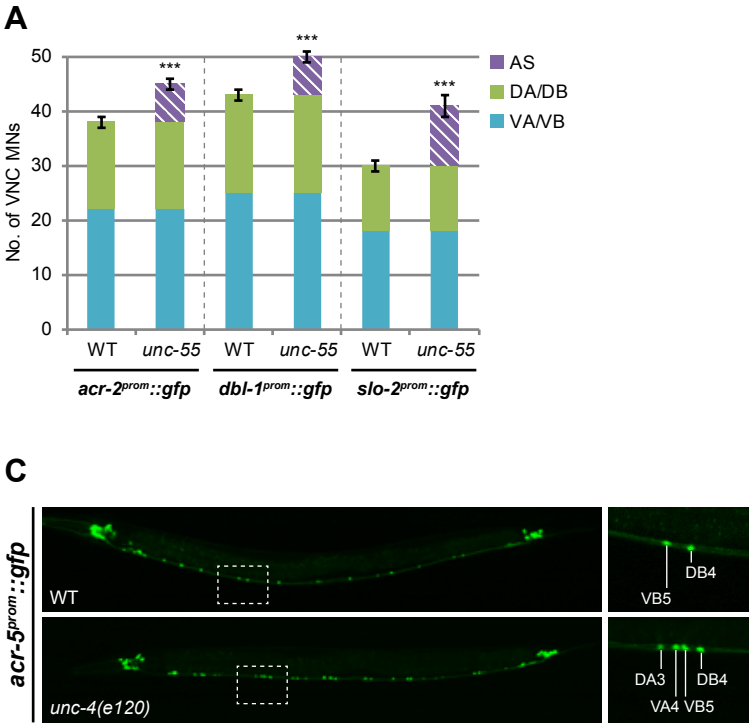
A
No. of VNC MNs
50
40
30
20
10
0
***
***
***
AS
DA/DB
VA/VB
WT
unc-55
WT
unc-55
WT
unc-55
acr-2prom::gfp
dbl-1prom::gfp
slo-2prom::gfp

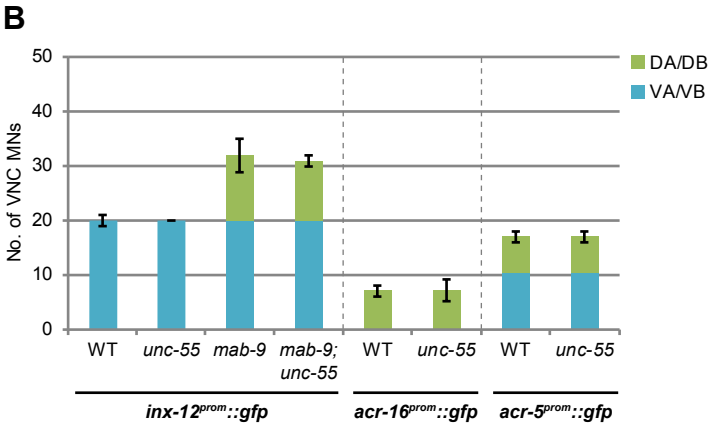
B
No. of VNC MNs
50
40
30
20
10
0
DA/DB
VA/VB
WT
unc-55
mab-9
mab-9; unc-55
WT
unc-55
WT
unc-55
inx-12prom::gfp
acr-16prom::gfp
acr-5prom::gfp

C
acr-5prom::gfp
WT
DB4
VB5
unc-4(e120)
DA3
DB4
VA4 VB5

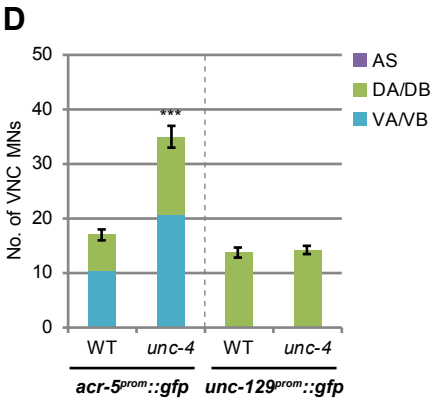
D
No. of VNC MNs
50
40
30
20
10
0
***
AS
DA/DB
VA/VB
WT
unc-4
WT
unc-4
acr-5prom::gfp
unc-129prom::gfp

Figure S4

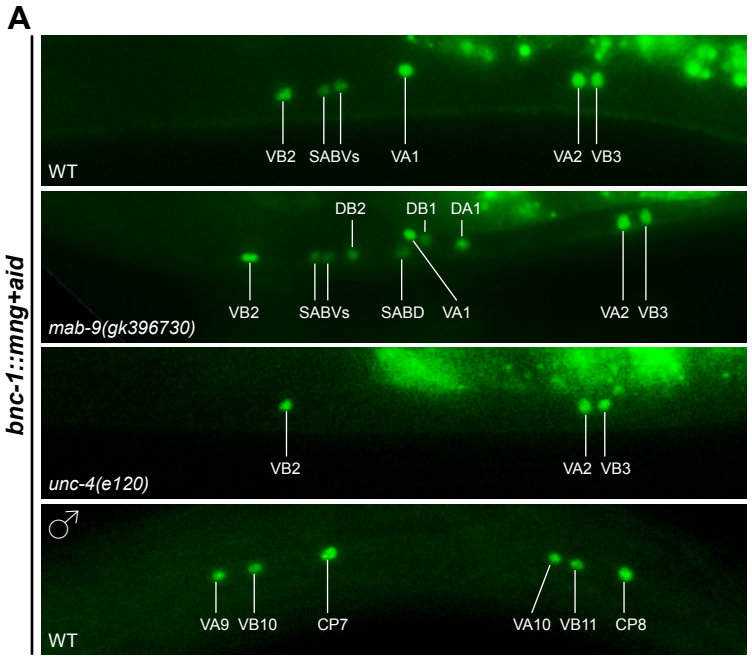
A
bnc-1::mng+aid
WT
VB2 SABVs VA1 VA2 VB3
mab-9(gk396730)
DB2 DB1 DA1
VB2 SABVs SABD VA1 VA2 VB3
unc-4(e120)
VB2 VA2 VB3
♂
WT
VA9 VB10 CP7 VA10 VB11 CP8

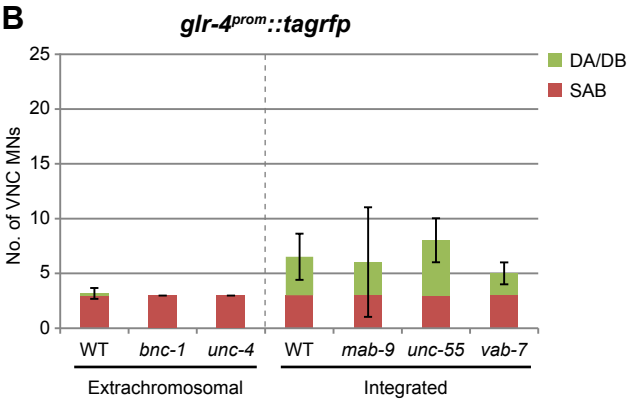
B
glr-4prom::tagrfp
DA/DB
SAB
No. of VNC MNs
0
5
10
15
20
25
WT bnc-1 unc-4
Extrachromosomal
WT mab-9 unc-55 vab-7
Integrated

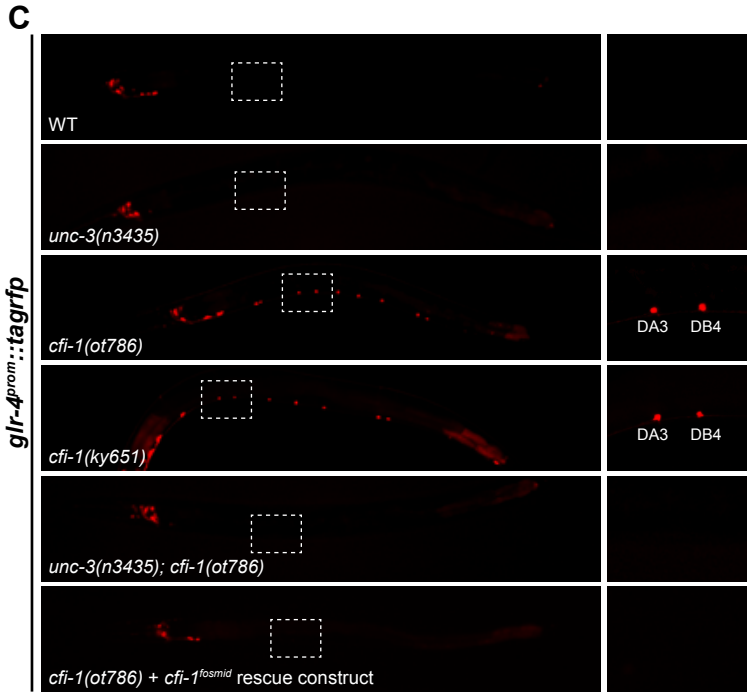
C
glr-4prom::tagrfp
WT
unc-3(n3435)
cfi-1(ot786)
DA3 DB4
cfi-1(ky651)
DA3 DB4
unc-3(n3435); cfi-1(ot786)
cfi-1(ot786) + cfi-1fosmid rescue construct

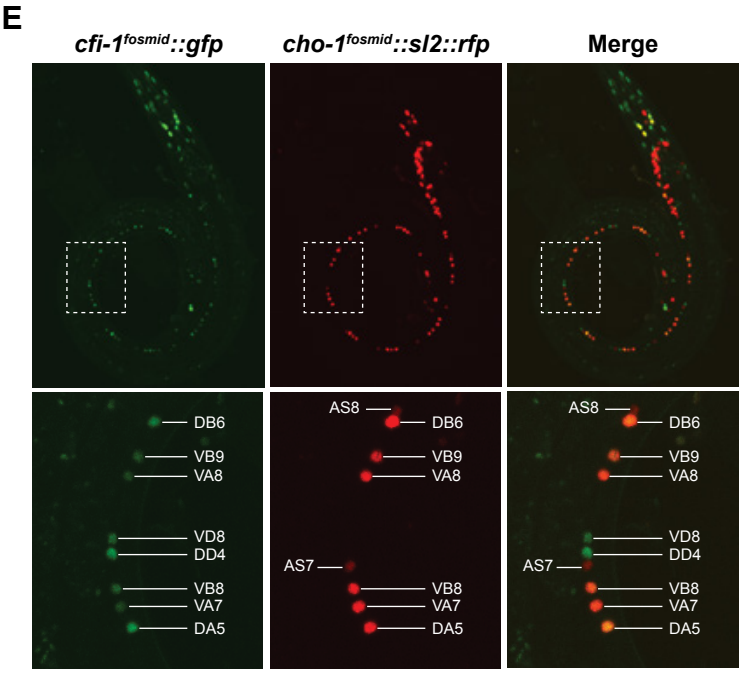
E
cfi-1fosmid::gfp
cho-1fosmid::sl2::rfp
Merge
DB6
VB9
VA8
VD8
DD4
VB8
VA7
DA5
AS8
AS7

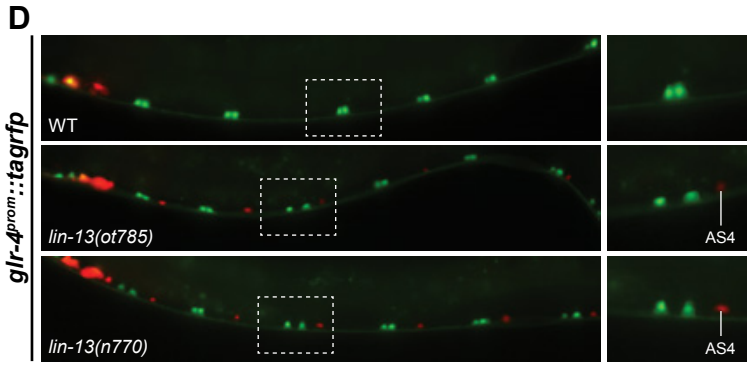
D
glr-4prom::tagrfp
WT
lin-13(ot785)
AS4
lin-13(n770)
AS4

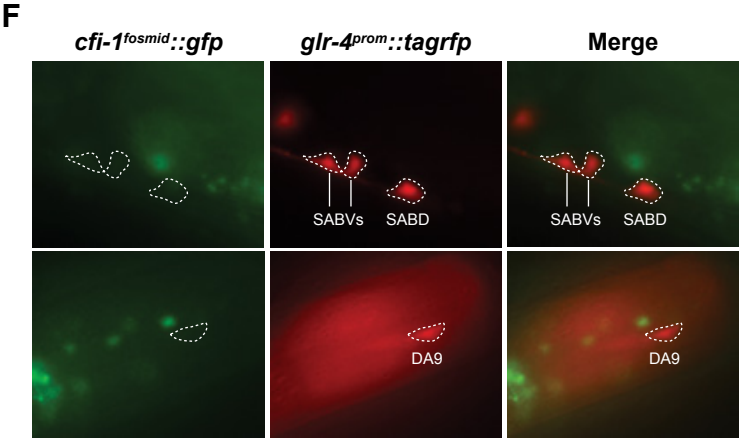
F
cfi-1fosmid::gfp
glr-4prom::tagrfp
Merge
SABVs SABD
DA9

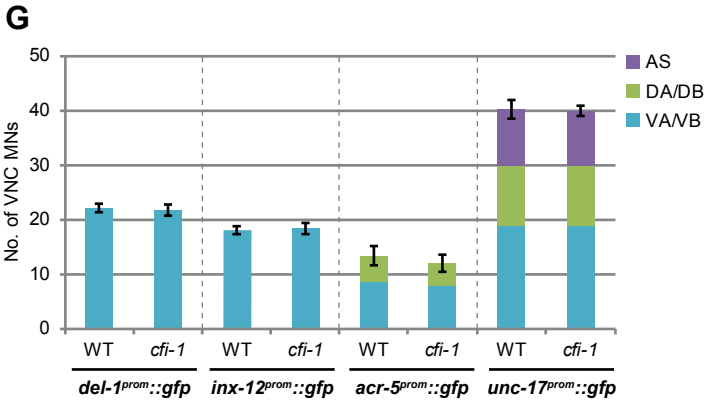
G
AS
DA/DB
VA/VB
No. of VNC MNs
0
10
20
30
40
50
WT cfi-1
del-1prom::gfp
WT cfi-1
inx-12prom::gfp
WT cfi-1
acr-5prom::gfp
WT cfi-1
unc-17prom::gfp

Figure S5

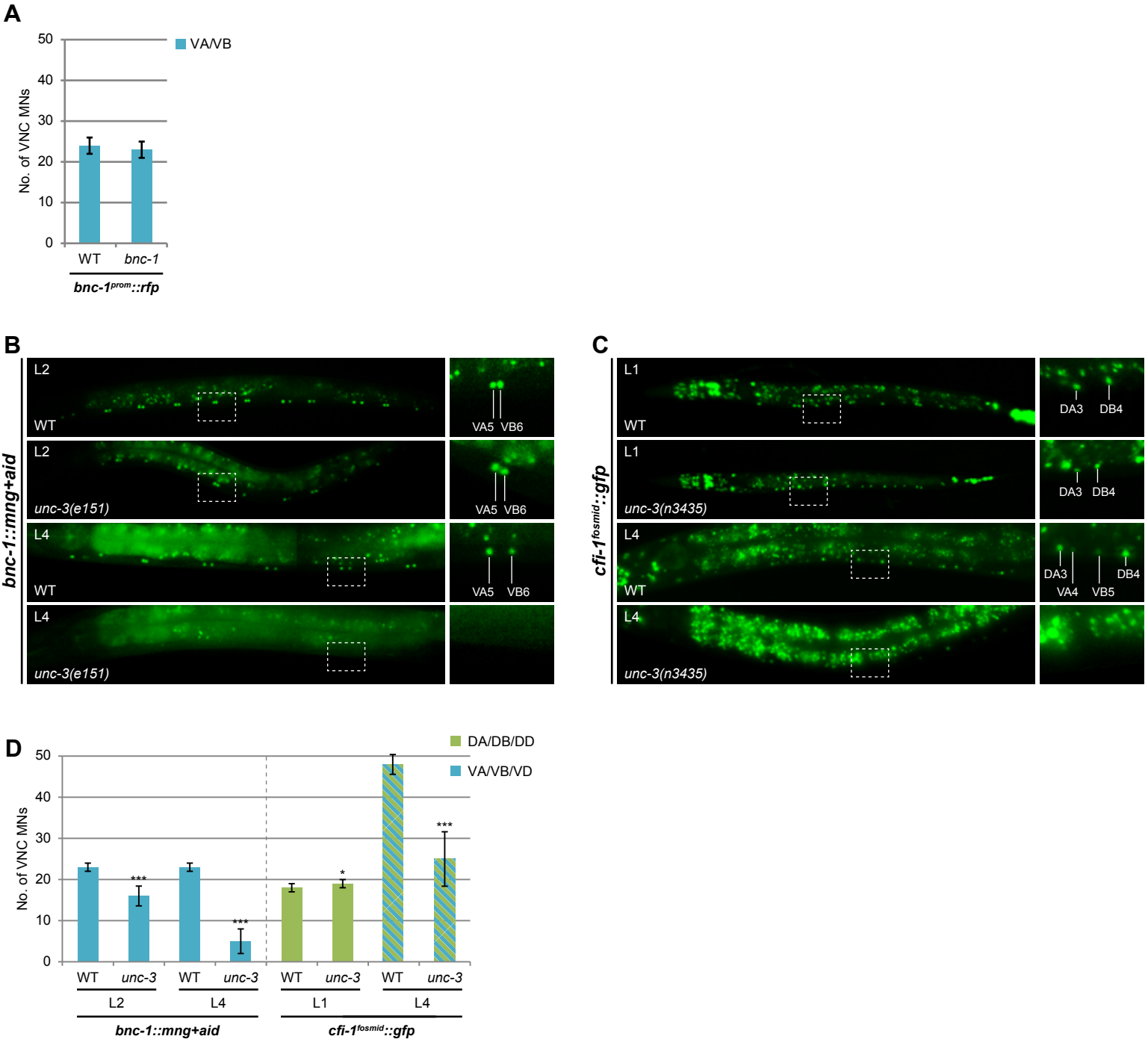
A
VA/VB
No. of VNC MNs
50
40
30
20
10
0
WT
bnc-1
bnc-1prom::rfp
B
bnc-1::mng+aid
L2
WT
VA5 VB6
L2
unc-3(e151)
VA5 VB6
L4
WT
VA5 VB6
L4
unc-3(e151)
C
cfi-1fosmid::gfp
L1
WT
DA3 DB4
L1
unc-3(n3435)
DA3 DB4
L4
WT
DA3 DB4
VA4 VB5
L4
unc-3(n3435)
D
DA/DB/DD
VA/VB/VD
No. of VNC MNs
50
40
30
20
10
0
***
***
*
***
WT
unc-3
WT
unc-3
WT
unc-3
WT
unc-3
L2
L4
L1
L4
bnc-1::mng+aid
cfi-1fosmid::gfp

Figure S6

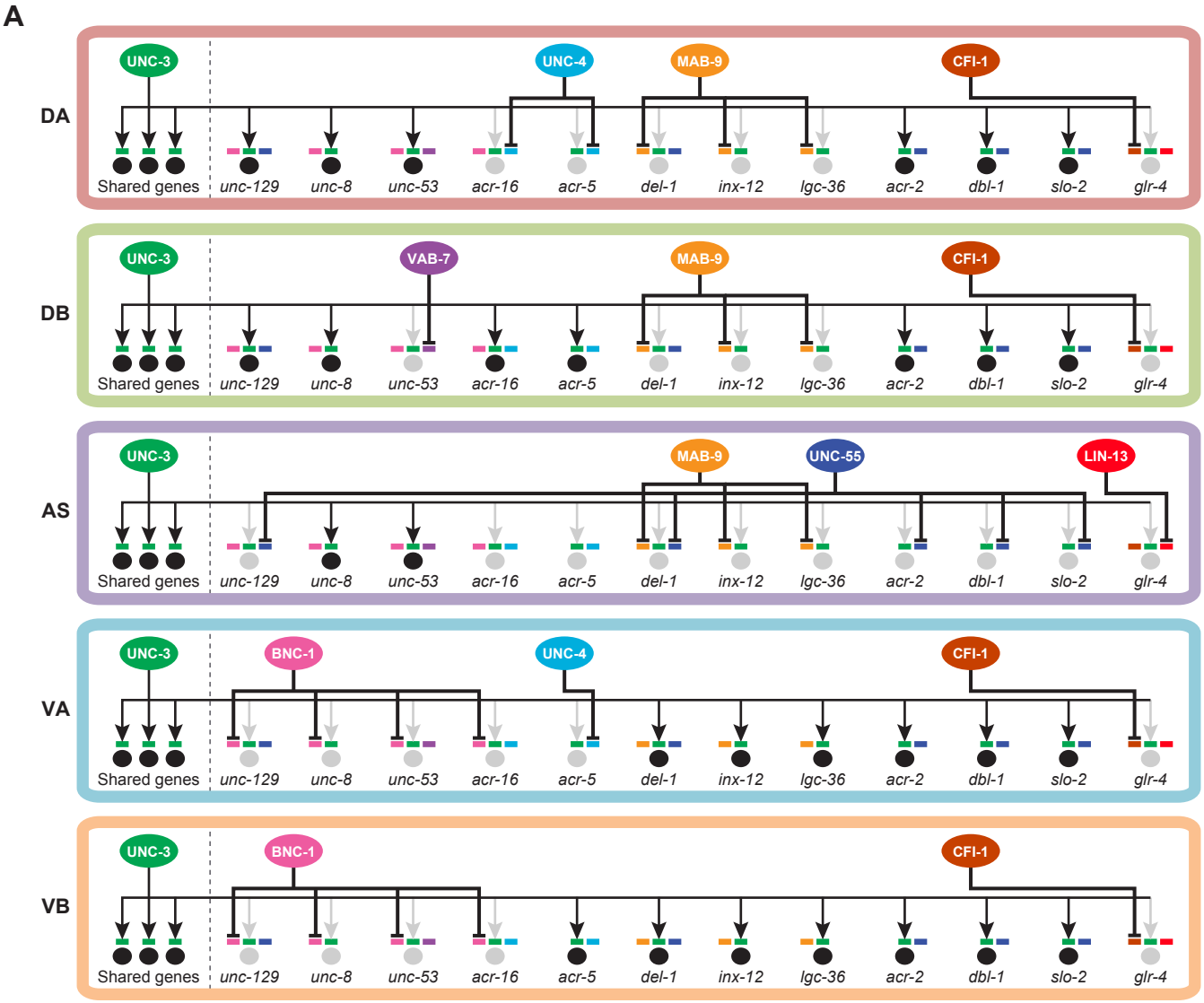
A
DA
UNC-3
UNC-4
MAB-9
CFI-1
Shared genes
unc-129
unc-8
unc-53
acr-16
acr-5
del-1
inx-12
lgc-36
acr-2
dbl-1
slo-2
glr-4
DB
UNC-3
VAB-7
MAB-9
CFI-1
Shared genes
unc-129
unc-8
unc-53
acr-16
acr-5
del-1
inx-12
lgc-36
acr-2
dbl-1
slo-2
glr-4
AS
UNC-3
MAB-9
UNC-55
LIN-13
Shared genes
unc-129
unc-8
unc-53
acr-16
acr-5
del-1
inx-12
lgc-36
acr-2
dbl-1
slo-2
glr-4
VA
UNC-3
BNC-1
UNC-4
CFI-1
Shared genes
unc-129
unc-8
unc-53
acr-16
acr-5
del-1
inx-12
lgc-36
acr-2
dbl-1
slo-2
glr-4
VB
UNC-3
BNC-1
CFI-1
Shared genes
unc-129
unc-8
unc-53
acr-16
acr-5
del-1
inx-12
lgc-36
acr-2
dbl-1
slo-2
glr-4

SUPPLEMENTAL FIGURE LEGENDS

Figure S1 (related to Fig.2,3): Additional characterization of *bnc-1* and *mab-9*

A: Quantification for **Fig.2F**; neurons in the RVG where this *unc-3* promoter expresses poorly were strictly excluded; error bars show SD. Identity of remaining VNC MNs where *unc-129* was not repressed by the *unc-3*^{prom}*::bnc-1* transgene could not be unambiguously ascertained as their positions seemed random and were thus binned together as D/V. Three independent transgenic lines were assessed (#1.1, #3.1, and #5.1). Unpaired *t*-tests were performed comparing each line with its corresponding no-transgene control and WT; ***$p < 0.001$; $n \geq 10$.

B: The expression of VA/VB-specific *del-1* and *inx-12*, DB/VB-specific *acr-5*, and cholinergic *unc-17* is not affected in *bnc-1* null mutants. Error bars show SD; $n \geq 13$.

C: The axonal morphology of VA/VB (which project ventrally) and DA/DB MNs (which project dorsally) is unaffected in, respectively, *bnc-1* and *mab-9* null mutants when compared to WT worms. The fluorophores of the reporter transgenes fill up the neuronal processes, allowing the axonal projections to be visualized. $n \geq 20$.

D: The distribution of presynaptic puncta of VA/VB (along the VNC) and DA/DB MNs (along the dorsal nerve cord) is unaffected in, respectively, *bnc-1* and *mab-9* null mutants when compared to WT worms. RAB-3 (a member of the Ras GTPase superfamily) is a presynaptic molecule which when translationally fused with a fluorophore, allows for the visualization of the presynapse of a neuron in which it is expressed. $n \geq 20$.

E: In *C. elegans*, cholinergic MNs in the VNC are dyadic, as they synapse onto muscle as well as GABAergic MNs. The distribution of postsynaptic puncta in GABAergic MNs of synapses originating from VA/VB (along the VNC) and DA/DB MNs (along the dorsal nerve cord) is unaffected in, respectively, *bnc-1* and *mab-9* null mutants when compared to WT worms. ACR-12 (an nAChR subunit) is a postsynaptic molecule which when translationally fused with a fluorophore, allows for the visualization of the postsynapse of the neuron in which it is expressed. In this case, the *unc-47* promoter drives ACR-12 expression in GABAergic MNs. All worm strains here are in the genetic background of *acr-12(ok367)* which is required for ACR-12+GFP to be detectable. $n \geq 20$.

F: The distribution of postsynaptic puncta in neuromuscular junctions (NMJ) originating from VA/VB (along the VNC) and DA/DB MNs (along the dorsal nerve cord) is unaffected in, respectively, *bnc-1* and *mab-9* null mutants when compared to WT worms. Here, the

endogenous *unc-29* locus (encoding an nAChR subunit that is a body wall muscle-specific postsynaptic molecule) is translationally fused with TagRFP to allow for the visualization of NMJ postsynapses. $n \geq 20$.

G: VA/VB-specific expression of the *bnc-1* translationally tagged fosmid (very dim but consistent) and transcriptionally tagged rescue construct reporters (as mentioned in **Fig.3E**).

H: Quantification for **Fig.3E**; error bars show SD. Unpaired *t*-tests were performed compared to WT; ***$p < 0.001$; $n \geq 13$.

I: Images of the *unc-3*-dependent, VA/VB-specific *lgc-36* (Gendrel *et al.*, 2016) being derepressed in DA/DB MNs in *mab-9* null mutants as quantified in **Fig.3G**. Showing anterior half of worm.

J: The expression of DB/VB-specific *acr-5* is not affected in *mab-9* null mutants. Error bars show SD; $n \geq 13$.

K: Quantification for *unc-3*^{prom}*::mab-9* transgenic line effect in **Fig.3A,F**; neurons in the RVG where this *unc-3* promoter expresses poorly were strictly excluded; error bars show SD. Identity of remaining VNC MNs where *del-1* was not repressed by the transgene could not be unambiguously ascertained as their positions seemed random and were thus binned together as D/V. At least two independent transgenic lines were assessed although only the most representative line is shown due to space constraints. Unpaired *t*-tests were performed comparing each line with its corresponding no-transgene control and WT; ***$p < 0.001$; $n \geq 10$.

Figure S2 (related to Fig.2,3): Identification of *bnc-1* and *mab-9* alleles

Hawaiian single nucleotide polymorphism (SNP) mapping plots obtained from whole-genome sequencing of the following repressor mutant alleles:

A: *bnc-1(ot721)*

B: *bnc-1(ot763)*

C: *mab-9(ot720)*

D: *mab-9(ot788)*

Figure S3 (related to Fig.4): Additional characterization of *unc-55* and *unc-4*

A: Quantification for **Fig.4C**; error bars show SD. Unpaired *t*-tests were performed compared to WT; ***$p < 0.001$; $n \geq 13$.

B: The expression of VA/VB-specific *inx-12*, DB-specific *acr-16*, and DB/VB-specific *acr-5* is not affected in *unc-55* null mutants. Expression of *inx-12* is also not affected in *mab-9;unc-55* double mutants (in contrast to VA/VB-specific *del-1*). Error bars show SD; $n \geq 13$.

C,D: In *unc-4* null mutants, DB/VB-specific *acr-5* is derepressed in DA/VA MNs. On the other hand, the expression of DA/DB-specific *unc-129* is not affected in *unc-4* null mutants. Error bars show SD; unpaired *t*-tests were performed compared to WT; ***$p < 0.001$; $n \geq 13$.

Figure S4 (related to Fig.5): Additional characterization of SAB motor neurons, *cfi-1* and *lin-13*

A: Besides VA/VB MNs, *bnc-1* is also expressed in the male-specific CP7 MN and CP8 interneuron in the VNC. Additionally, *bnc-1* is expressed dimly in SABVs in the RVG. In *mab-9* null mutants, *bnc-1* is derepressed in SABD. In *unc-4* null mutants, *bnc-1* in SABVs is lost, presumably due to the derepression of *mab-9* which otherwise represses *bnc-1* (see **Fig.5E** for genetic model).

B: The expression of SAB-specific *glr-4* is not affected in *bnc-1*, *unc-4*, *mab-9*, *unc-55*, and *vab-7* null mutants. The integrated strain (first shown in **Fig.5F**) is derived from the extrachromosomal strain (first shown in **Fig.6I**). Error bars show SD; $n \geq 13$.

C: Images of the SAB-specific *glr-4* being derepressed in DA/DB MNs in *cfi-1* null mutants in an *unc-3*-dependent manner as quantified in **Fig.5F**. That glr-4 expression is largely absent from the VNC is independently corroborated by the translational reporter transgene *akEx32[glr-4::gfp]*. For the fosmid rescue experiment, three independent transgenic lines were assessed although only the most representative line is shown due to space constraints.

D: Images of the SAB-specific *glr-4* being derepressed in AS MNs in *lin-13* null mutants as quantified in **Fig.5F**. Due to its very broad expression and its colocalization and physical association with the *C. elegans* ortholog of heterochromatin protein 1 (HP1), *lin-13* is thought to be a general corepressor of gene expression (Coustham *et al.*, 2006; Grant *et al.*, 2010) and we did not pursue its characterization further.

E: *cfi-1* is expressed in DA/DB/VA/VB/DD/VD but not in AS MNs in the VNC.

F: *cfi-1* is also not expressed in SAB MNs in the RVG or in DA9 MNs in the preanal ganglion (PAG).

G: The expression of VA/VB-specific *del-1* and *inx-12*, DB/VB-specific *acr-5*, and cholinergic *unc-17* is not affected in *cfi-1* null mutants. For the latter three, MNs in the RVG and PAG were not quantified. Error bars show SD; $n \geq 10$.

Figure S5 (related to Fig.7): *unc-3* maintains but does not initiate *bnc-1* and *cfi-1* expression

A: The VA/VB-specific expression driven by the *bnc-1* promoter is not affected in *bnc-1* null mutants – indicating that *bnc-1* does not auto-regulate. Error bars show SD; n ≥ 13.

B: In *unc-3* null mutants, the VA/VB-specific expression of *bnc-1* is observed (albeit less consistently) at the L2 stage but is lost by the L4 stage. This indicates a requirement of UNC-3 to postdevelopmentally maintain but not to initiate *bnc-1* expression. VA/VB MNs are generated at the late L1 stage. L4 WT image repeated from **Fig.2E**.

C: In *unc-3* null mutants compared to WT, *cfi-1* expression is observed in VNC MNs at the L1 stage but is considerably lost by the L4 stage. This indicates a requirement of UNC-3 to postdevelopmentally maintain but not to initiate *cfi-1* expression. Only DA/DB/DD MNs have been generated by the L1 stage while VA/VB/VD MNs are generated at the late L1 stage. The remaining VNC MNs in the *unc-3* mutant at the L4 stage are presumably the DD/VD MNs which do not express *unc-3*.

D: Quantification for **C** and **D**; error bars show SD. Unpaired *t*-tests were performed compared to WT; ***$p < 0.001$; *$p < 0.05$; $n \geq 13$.
Note: Worm strains of *unc-3(ot837)* crossed with *evIs82B* or *wdIs3* are slightly uncoordinated, a phenotype not observed in these strains by themselves.

Figure S6 (related to Fig.8): Detailed model

A: Model of neuron identity diversification (similar to **Fig.8B** but with results from this study incorporated) depicting the transcriptional activity of a broadly acting terminal selector (*e.g.* UNC-3 specifying cholinergic MNs) being counteracted upon by subtype-specific repressors (*e.g.* the repressors uncovered in this study) at the target effector gene level.

SUPPLEMENTARY TABLES

Table S1 (related to Fig.6 and Experimental Procedures): Transcription factor binding site prediction and mutation

Table S2 (related to Experimental Procedures): New transgenic alleles and information on their generation

Table S1 (related to Fig.6 and Experimental Procedures): Transcription factor binding site prediction and mutation

Transcription factor	Binding site consensus motif	Method and reference	Effector gene search target	Binding site sequence and mutation	*Caenorhabditis* species conservation
C. elegans UNC-3		Generated from Kratsios *et al.* (2011)	*acr-16*	TCTCCAGAGG ↓ TGGCCAGAGG	3 other species
C. elegans BNC-1		PBM; Narasimhan *et al.* (2015)	*unc-129*	TGTCACCTT ↓ AAGAGCCTT	5 other species
			acr-16	TGTCACCAG ↓ AAGAGCCAG	3 other species
D. melanogaster Mid (MAB-9)	DRRGTGWBRARGCG (allow 1 mismatch)	SELEX; Najand *et al.* (2012)	*bnc-1*	AGGGTGTCGAAGTG ↓ (24 bp deletion)	5 other species
M. musculus Tbx20 (MAB-9)		PBM; Weirauch *et al.* (2013)		GAAGTGTGAA ↓ (24 bp deletion)	5 other species
H. sapiens TBX20		SELEX; Jolma *et al.* (2013)		GGGTGTCGAAGTGTGA ↓ (24 bp deletion)	5 other species
M. musculus Tbx20	AGGTGTGA (allow 2 mismatches)	SELEX; Macindoe *et al.* (2009)	*del-1*	(i) AAATGTGAAACG ↓ AAAACCCCCTTT	3 other species
M. musculus Tbx20		ChIP-seq; Shen *et al.* (2011)	*del-1*	(ii) ACTTGATGAAAG ↓ ACTTCCCCCCCC	0 other species

C. elegans nuclear hormone receptors (UNC-55)	TGACCT (allow 1 mismatch)	Reviewed in Van Gilst *et al.* (2002)	*unc-129*	ATGTCACCTT ↓ TAAGAGCCTT	5 other species
			del-1	(i) TGAACT ↓ CCCACT	2 other species
				(ii) TGCCCT ↓ TTTAAA	1 other species
M. musculus Nr2f1 (UNC-55)		PBM; Weirauch *et al.* (2013)	*del-1*	(iii) GTGCCCTT ↓ GCAAAACT	0 other species
				(iv) ATGACCTG ↓ AGTTTTGG	0 other species
M. musculus Arid3a (CFI-1)		ChIP-seq; Rhee *et al.* (2014)	*glr-4*	(i) ATTTTTAT ↓ (28 bp deletion)	3 other species
C. elegans CFI-1	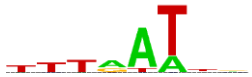	PBM; Weirauch *et al.* (2014)	*glr-4*	(ii) TTTGATAT ↓ (8 bp deletion)	6 other species
				(iii) TTTGATTG ↓ (8 bp deletion)	6 other species
				(iv) TTTGATTT ↓ (14 bp deletion)	5 other species

Note:
Red letters indicate mutated sequences. See **Table S2** for precise positions of deletion mutations.

SUPPLEMENTAL EXPERIMENTAL PROCEDURES

Mutant strains

The *C. elegans* mutant alleles <strain name> used in this study were: *unc-3(e151)* <CB151>, *unc-3(n3435)* <MT10785>, *unc-3(ot837[unc-3::mng+aid])* <OH13988>, *bnc-1(ot721)* <OH14045>, *bnc-1(ot763)* <OH14044>, *bnc-1(ot845[bnc-1::mng+aid])* <OH14070>, *mab-9(e2410)* <CB4605>, *mab-9(gk396730)* <VC20768>, *mab-9(ot720)* <OH11850>, *mab-9(ot788)* <OH12389>, *mab-9(ot863[mab-9::TagRFP+aid])* <OH14357>, *unc-55(e402)* <CB402>, *unc-55(e1170)* <CB1170>, *unc-55(ot718)* <OH11837>, *unc-4(e26)* <NC168>, *unc-4(e120)* <CB120>, *unc-4(e2322ts)* <NC37>, *vab-7(e1562)* <CB1562>, *cfi-1(ky651)* <OS122>, *cfi-1(ot786)* <OH12344>, *lin-13(n770)* <MT8838>, *lin-13(ot785)* <OH12343>, *acr-12(ok367)* <IZ1225>, and *unc-29(kr208[unc-29::TagRFP])* <OH12325>.

Transgenic strains

The *C. elegans* transgenic alleles <strain name> used in this study that have been published were *evIs82B[unc-129^{prom}::gfp]* <OH4128>, *hdIs1[unc-53^{prom}::gfp]* <VH111>, *wdEx419[acr-16^{prom}::gfp]* <NC972>, *wdIs3[del-1^{prom}::gfp]* <NC138>, *wdIs6[del-1^{prom}::gfp]* <NC190>, *zwEx112[inx-12^{prom}::gfp]* <ZW292>, *otEx6844[lgc-36^{fosmid}::sl2::yfp]* <OH14644>; *juIs14[acr-2^{prom}::gfp]* <CZ631>, *ctIs43[dbl-1^{prom}::gfp]* <BW1935>, *sEx10749[slo-2^{prom}::gfp]* <BC10749>, *wdEx75[acr-5^{prom}::gfp]* <NC216>, *akEx32[glr-4::gfp]* <VM141>, *otIs476[glr-4^{prom}::TagRFP]* <OH12052>, *vsIs48[unc-17^{prom}::gfp]* <LX929>, *ieSi57[eft-3^{prom}::tir1]* <CA1200>, *ufIs92[unc-47^{prom}::acr-12+gfp]* <IZ1225>, and *otIs544[cho-1^{fosmid}::sl2::rfp]* <OH12655>. See **Table S2** for new transgenic alleles used in this study with detailed information on their generation. The fosmid of clone WRM0624cC09 in which the *bnc-1* gene locus was translationally fused with green fluorescent protein (GFP) just before the stop codon was kindly provided by the *C. elegans* Transgeneome Project (Sarov *et al.*, 2012). Recombineering of the fosmid clone WRM0614dC10 in which the *cfi-1* gene locus was translationally fused with GFP just before the stop codon was performed exactly as described in Tursun *et al.*, (2009).

Forward genetic screens

EMS mutagenesis was separately performed on three fluorescent reporter strains: *evIs82B[unc-129^{prom}::gfp]*, *hdIs1[unc-53^{prom}::gfp]*, and *otIs476[glr-4^{prom}::TagRFP]*, before manually screening for changes in reporter expression in VNC MNs. Automated screening for loss of reporter expression in VNC MNs was also performed on *evIs82B* using the Union Biometrica Copas Biosort system (Doitsidou *et al.*, 2008). To identify the causal genes of the mutant alleles obtained, Hawaiian single nucleotide polymorphism (SNP) mapping and whole-genome sequencing (Doitsidou *et al.*, 2010) were performed followed by data analysis using the CloudMap pipeline (Minevich *et al.*, 2012). In addition to those reported in the Results section, mutant alleles of the following genes were also identified: *unc-3(ot722)*, *unc-3(ot789)*, and *ref-2(ot762)*.

Targeted genome modification

The CRISPR/Cas9-mediated modification of the genome to, separately, translationally fuse the *unc-3*, *bnc-1*, and *mab-9* gene loci with the fluorescent reporter mNeonGreen (mNG) followed by the auxin-inducible degron (AID) just before the stop codon was performed exactly as described in Dickinson *et al.*, 2015.

Microscopy

Worms were anesthetized using 100 mM sodium azide (NaN_3) and mounted on 5% agarose pads on glass slides. Images were acquired as Z-stacks of ~1 µm-thick slices with the Micro-Manager software (Edelstein *et al.*, 2010) using the Zeiss Axio Imager.Z1 automated fluorescence microscope. Images were reconstructed via maximum intensity Z-projection of 2-10 µm Z-stacks using the ImageJ software (Schneider *et al.*, 2012).

SUPPLEMENTAL REFERENCES

Coustham, V., Bedet, C., Monier, K., Schott, S., Karali, M., and Palladino, F. (2006). The C. elegans HP1 homologue HPL-2 and the LIN-13 zinc finger protein form a complex implicated in vulval development. Dev Biol *297*, 308-322.

Dickinson, D.J., Pani, A.M., Heppert, J.K., Higgins, C.D., and Goldstein, B. (2015). Streamlined Genome Engineering with a Self-Excising Drug Selection Cassette. Genetics *200*, 1035-1049.

Doitsidou, M., Flames, N., Lee, A.C., Boyanov, A., and Hobert, O. (2008). Automated screening for mutants affecting dopaminergic-neuron specification in C. elegans. Nat Methods *5*, 869-872.

Doitsidou, M., Poole, R.J., Sarin, S., Bigelow, H., and Hobert, O. (2010). C. elegans mutant identification with a one-step whole-genome-sequencing and SNP mapping strategy. PLoS One *5*, e15435.

Edelstein, A., Amodaj, N., Hoover, K., Vale, R., and Stuurman, N. (2010). Computer control of microscopes using microManager. Curr Protoc Mol Biol *Chapter 14*, Unit14 20.

Gendrel, M., Atlas, E.G., and Hobert, O. (2016). A cellular and regulatory map of the GABAergic nervous system of C. elegans. Elife *5*.

Grant, J., Verrill, C., Coustham, V., Arneodo, A., Palladino, F., Monier, K., and Khalil, A. (2010). Perinuclear distribution of heterochromatin in developing C. elegans embryos. Chromosome Res *18*, 873-885.

Jolma, A., Yan, J., Whitington, T., Toivonen, J., Nitta, K.R., Rastas, P., Morgunova, E., Enge, M., Taipale, M., Wei, G.*, et al.* (2013). DNA-binding specificities of human transcription factors. Cell *152*, 327-339.

Macindoe, I., Glockner, L., Vukasin, P., Stennard, F.A., Costa, M.W., Harvey, R.P., Mackay, J.P., and Sunde, M. (2009). Conformational stability and DNA binding specificity of the cardiac T-box transcription factor Tbx20. J Mol Biol *389*, 606-618.

Minevich, G., Park, D.S., Blankenberg, D., Poole, R.J., and Hobert, O. (2012). CloudMap: a cloud-based pipeline for analysis of mutant genome sequences. Genetics *192*, 1249-1269.

Najand, N., Ryu, J.R., and Brook, W.J. (2012). In vitro site selection of a consensus binding site for the Drosophila melanogaster Tbx20 homolog midline. PLoS One *7*, e48176.

Narasimhan, K., Lambert, S.A., Yang, A.W., Riddell, J., Mnaimneh, S., Zheng, H., Albu, M., Najafabadi, H.S., Reece-Hoyes, J.S., Fuxman Bass, J.I.*, et al.* (2015). Mapping and analysis of Caenorhabditis elegans transcription factor sequence specificities. Elife *4*.

Rhee, C., Lee, B.K., Beck, S., Anjum, A., Cook, K.R., Popowski, M., Tucker, H.O., and Kim, J. (2014). Arid3a is essential to execution of the first cell fate decision via direct embryonic and extraembryonic transcriptional regulation. Genes Dev *28*, 2219-2232.

Sarov, M., Murray, J.I., Schanze, K., Pozniakovski, A., Niu, W., Angermann, K., Hasse, S., Rupprecht, M., Vinis, E., Tinney, M.*, et al.* (2012). A genome-scale resource for in vivo tag-based protein function exploration in C. elegans. Cell *150*, 855-866.

Schneider, C.A., Rasband, W.S., and Eliceiri, K.W. (2012). NIH Image to ImageJ: 25 years of image analysis. Nat Methods *9*, 671-675.

Shen, T., Aneas, I., Sakabe, N., Dirschinger, R.J., Wang, G., Smemo, S., Westlund, J.M., Cheng, H., Dalton, N., Gu, Y.*, et al.* (2011). Tbx20 regulates a genetic program essential to adult mouse cardiomyocyte function. J Clin Invest *121*, 4640-4654.

Tursun, B., Cochella, L., Carrera, I., and Hobert, O. (2009). A toolkit and robust pipeline for the generation of fosmid-based reporter genes in C. elegans. PLoS One *4*, e4625.

Van Gilst, M., Gissendanner, C.R., and Sluder, A.E. (2002). Diversity and function of orphan nuclear receptors in nematodes. Crit Rev Eukaryot Gene Expr *12*, 65-88.

Weirauch, M.T., Cote, A., Norel, R., Annala, M., Zhao, Y., Riley, T.R., Saez-Rodriguez, J., Cokelaer, T., Vedenko, A., Talukder, S.*, et al.* (2013). Evaluation of methods for modeling transcription factor sequence specificity. Nat Biotechnol *31*, 126-134.